

Hybrid optomechanical superconducting qubit system

Juuso Manninen,¹ Robert H. Blick,^{2,3} and Francesco Massel^{1,*}

¹*Department of Science and Industry Systems, University of South-Eastern Norway, PO Box 235, Kongsberg, Norway*

²*Center for Hybrid Nanostructures (CHyN), Universität Hamburg,
Luruper Chaussee 149, Hamburg 22761 Germany*

³*Materials Science and Engineering, University of Wisconsin-Madison, 1509 University Ave. WI 53706 U.S.A.*

(Dated: February 29, 2024)

We propose an integrated nonlinear superconducting device based on a nanoelectromechanical shuttle. The system can be described as a qubit coupled to a bosonic mode. The topology of the circuit gives rise to an adjustable qubit/mechanical coupling, allowing the experimenter to tune between linear and quadratic coupling in the mechanical degrees of freedom. Owing to its flexibility and potential scalability, the proposed setup represents an important step towards the implementation of bosonic error correction with mechanical elements in large-scale superconducting circuits. We give preliminary evidence of this possibility by discussing a simple state-swapping protocol that uses this device as a quantum memory element.

I. INTRODUCTION

In recent years, optomechanical systems, both in the optical and in the microwave regime, have become one of the most prominent platforms for the investigation of quantum mechanical phenomena. On the one hand, they have allowed scientists to explore foundational aspects of quantum theory [1, 2]; on the other, they have provided the test bed for future technological applications of quantum mechanics [3]. Prominent results in the field include sideband [4] and feedback [5] cooling to the ground state, squeezing [6, 7], and entanglement [8, 9] of mechanical resonators. In the context of coupling between qubits and mechanical resonators, the generation of quantum states of mechanical motion has been recently realized in high-overtone bulk acoustic-wave resonators (HBARs) where the generation of Fock [10] and cat [11] states were demonstrated.

In most of the examples mentioned above, the optomechanical system consists of a mechanical resonator (e.g. a nano-drum) whose position is parametrically coupled to a photon cavity. One of the outstanding goals in these systems has been the realization of the so-called single-photon strong-coupling limit. In this regime, the parametric coupling energy between a single photon and the mechanical mode becomes comparable to the bare optical cavity linewidth and can therefore significantly alter the dynamics of the system [12–20]. In microwave setups, several proposals suggest that the addition of nonlinear elements, in the form of Josephson junctions, can provide the resource needed to reach the strong-coupling regime; realizations along these lines include charge [12, 21] and flux-mediated optomechanical circuits [22].

Another intriguing aspect of these systems is the possibility of realizing a quadratic coupling between the mechanical motion and the optical field. Arguably, its most prominent application is the detection of phonon

Fock states [23–27], even though two-photon cooling and squeezing both of the mechanical and the electromagnetic degrees of freedom have been predicted [27] as well. In the optical frequencies range, the quadratic coupling of an optical cavity with a mechanical mode has been realized, e.g. in membrane-in-the-middle [23] and ultracold gases setups [28]. In the microwave regime, quadratic parametric coupling of a qubit to mechanical motion was recently realized with drumhead mechanical resonators coupled to superconducting circuits, exploiting the large mismatch of mechanical and qubit resonant frequency [29, 30], where the generation of (non-Gaussian) number-squeezed states was demonstrated.

In this work, we extend the nonlinear circuit approaches mentioned above, integrating a mechanical shuttling element into the design of the superconducting circuit of Fig. 1. The shuttling element consists here of a portion of superconducting material that is free to perform mechanical oscillations between two (superconducting) electrodes. Analogous shuttling devices were realized experimentally in normal (i.e. non superconducting) circuits [31–33], demonstrating the ability of such devices to “shuttle” electrons along with the oscillatory mechanical motion. In addition, an analogous shuttling mechanism for Cooper pairs was theoretically investigated for superconducting circuits [34]. In our work, we explore how the dynamical properties of a superconducting shuttling element can be recast in terms of a (nonlinear) optomechanical coupling between a superconducting circuit and a mechanical mode, for which we believe this particular charge shuttling mechanism certainly offers a new degree of freedom [35].

More specifically, we show how, in a lumped-element description, we are able to define a system constituted by a superconducting qubit exhibiting an intrinsic quadratic coupling to the mechanical motion, in addition to a tunable linear one. The latter can be externally suppressed, leading to a dominant coupling that is quadratic in the mechanical degrees of freedom. At the same time, we will show that the tunability of the linear coupling term allows for a coherent state exchange between the qubit

arXiv:2402.18317v1 [quant-ph] 28 Feb 2024

* francesco.massel@usn.no

and the mechanical resonator.

II. THE DEVICE

Our device is constituted by a superconducting shuttle, which is free to oscillate between two terminals, as shown in Fig. 1. The terminals being gated to a voltage source V_g through a gating capacitance C_g . The addition of a shunting capacitance C_b , meant to ensure protection from charge fluctuations, defines a transmon qubit-like device [36] (the X2MON) exhibiting nontrivial properties as a function of the mechanical shuttle dynamics. The displacement of the grounded island induces a shift in the Josephson and charging energies of the two Josephson junctions (JJs), which translates into a coupling between the superconducting circuit and the mechanical motion. As anticipated, in our device, the coupling between the mechanical degrees of freedom and a superconducting qubit can be externally tuned between a *linear* and a *quadratic* coupling, depending on the external magnetic flux through the loop defined by the two JJs. The setup we propose here differs from the design of Refs. [29, 30] inasmuch our realization, for suitable values of the control parameter, is *intrinsically* quadratic in the mechanical displacement –i.e. not relying on the relative value of the mechanical and qubit frequencies– owing to the symmetry of the design.

From a quantum-computational perspective, the coupling between a qubit and a bosonic mode –represented here, as we will show, by a shuttling mechanical element– is an extremely promising candidate for quantum error correction [37, 38]. Most importantly, the tunability of the qubit/mechanical coupling of our setup allows for a great flexibility in the choice of different protocols for state-preparation and state-transfer between qubit and mechanics. Further advantages offered by mechanical resonators compared to microwave cavities as the bosonic mode are represented by their larger coherence times (mechanical linewidths ~ 1 kHz [32] vs. cavity linewidths ~ 100 kHz), the lack of “cross-talk” between the bosonic (mechanical) modes and, with specific reference to shuttling mechanical elements, the scalability of such platforms.

A. Lumped-element model

Following Koch *et al.* [36], we describe the Josephson junction energy as the sum of a capacitive contribution E_C and the Josephson energy E_J . In our device, the lower portion of the circuit –the orange element in Fig. 1– corresponds to the actual island. As a consequence, the charging and Josephson energies become dependent on the shuttle dynamics $E_{C1,2} = E_{C1,2}(x_0 \pm \delta)$, $E_{J1,2} = E_{J1,2}(x_0 \pm \delta)$. Owing to the symmetry of the device, the upper (lower) sign corresponds to junction 1 (junction 2).

The total charging energy for the circuit can be written as

$$E_C = \frac{e^2}{2C_\Sigma} \quad (1)$$

with $C_\Sigma = C_{J1} + C_{J2} + C_b + C_g$ where C_{J1} and C_{J2} are the capacitances of the two Josephson junctions, C_g the gate capacitance and C_b the shunting capacitance aimed at reducing the effects of charge noise, like in a conventional transmon setup.

In the following, we will assume that the geometric capacitances associated with the Josephson junctions C_{J1} and C_{J2} can be modeled by two (equal, parallel plate) capacitors $C_{J1,2} \doteq C_J / (1 \pm \delta/x_0)$. Furthermore, we assume an exponential dependence of E_J on the electrodes’ separation. This assumption can be justified through the standard Ambegaokar-Baratoff formula [39, 40] arguing that the normal-state resistance is given by $R_N = R_{N0} \exp[x/\xi]$, (x thickness of the JJ), as a consequence of the exponential suppression of the tunneling probability through a potential barrier, combined with the Landauer formula [41], leading to

$$E_{J1,2} = E_J \exp \left[\mp \frac{\delta}{\xi} \right] \quad (2)$$

with $\xi = x_0 / \log \left[\frac{\Delta R_K}{8E_J R_{N0}} \right]$ and $E_J = E_{J1}(0) = E_{J2}(0)$ for symmetrical JJs. Here Δ is the superconducting gap and $R_K = 2\pi\hbar/e^2$ the resistance quantum. For a typical NbN junction, we can assume $\Delta = 4500$ GHz, $E_J = 20$ GHz, $R_{N0} = 50 \Omega$, and $x_0 = 1$ nm, allowing us to estimate $\xi \simeq 0.1$ nm ($\hbar = 1$ throughout the manuscript). Following Ref. [36], we can write the system’s Hamiltonian as

$$H = 4E_C(\delta)(n - n_g)^2 - E_\Sigma(\delta) \cos\left(\frac{\phi_b}{2}\right) \cos(\phi) - E_\Delta(\delta) \sin\left(\frac{\phi_b}{2}\right) \sin(\phi) + E(x_m, p_m), \quad (3)$$

where n and ϕ are the excess number of charge carriers and phase on the island, respectively, and $E_\Sigma(\delta) = E_{J1}(\delta) + E_{J2}(\delta)$, $E_\Delta(\delta) = E_{J1}(\delta) - E_{J2}(\delta)$. For a symmetric setup, we have

$$E_\Sigma(\delta) = 2E_J \cosh\left(\frac{\delta}{\xi}\right) \quad (4a)$$

$$E_\Delta(\delta) = 2E_J \sinh\left(\frac{\delta}{\xi}\right), \quad (4b)$$

where E_J is the Josephson energy associated with either junction. Furthermore, n_g is related to the external bias voltage by $n_g = -C_g V_g / 2e$ and the phase ϕ_b is determined by the external flux bias $\Phi_b = \Phi_0 / 2\pi \phi_b$ through the loop defined by the two JJs ($\Phi_0 = h/2e$). Here, the JJs are assumed to be symmetrical, but the full calculation with general junctions is presented in the Supplemental Material. Finally, the term $E(x_m, p_m)$ in the energy associated with the dynamics of the center of mass of

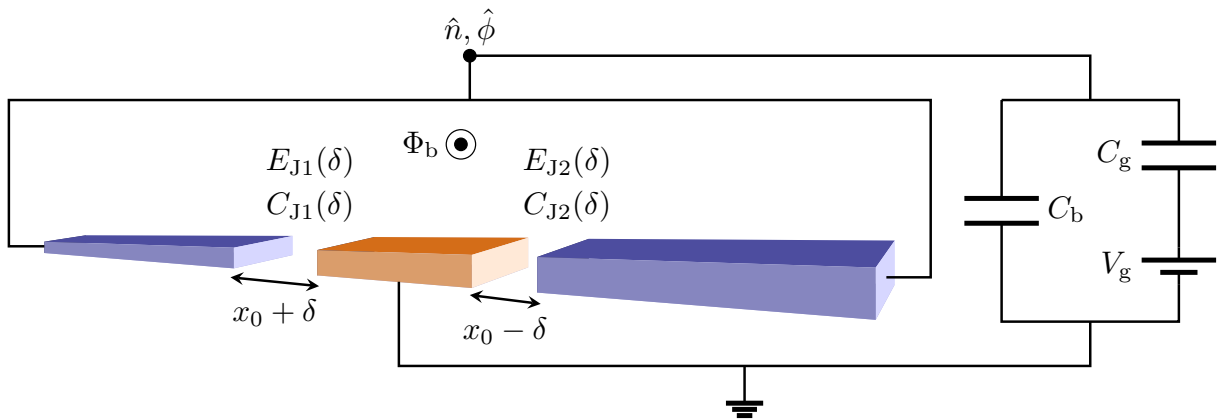


FIG. 1. Cartoon picture of a (grounded) X2MON shuttle and a lumped-element description of a transmon-like setup, including the X2MON. Contacts between the shuttle (orange) and its terminals (blue) can be described by position-dependent Josephson junctions.

the shuttle, which, in our analysis, we model as a simple harmonic oscillator.

Expanding the Hamiltonian given in Eq. (3) in powers of $\hat{\phi}$ up to the fourth order and in powers of the mechanical displacement up to the second order, focusing on the two lowest-charge states we have (see e.g. [42])

$$H = \frac{\omega_q}{2} \sigma_z + \omega_m b^\dagger b + g_1 (b^\dagger + b) \sigma_x + g_2 (b^\dagger + b)^2 \sigma_z \quad (5)$$

where $\sigma_z = 2a^\dagger a - 1$, $\sigma_x = a^\dagger + a$. The operators a (a^\dagger), b (b^\dagger) are the lowering (raising) operators associated with the electrical and mechanical degrees of freedom, respectively. All coefficients in Eq. (5) (ω_q , ω_m , g_1 , g_2) depend on the external flux bias. The explicit dependence on Φ_b is given in the Supplemental Material. As shown in Fig. 2, g_2 is the dominating interaction when the bias flux through the JJ loop is set to zero, since g_1 vanishes in this case. However, g_1 becomes the dominating term even for small deviations from the $\Phi_b = 0$ condition. As we will show below, this ability to control the type of interaction between the qubit and the mechanics makes this system very flexible in terms of possible applications, such as preparing the mechanical oscillator into a specific quantum state. For $m \simeq 5 \cdot 10^{-19}$ kg, $\omega_m = 1$ GHz, and $\omega_q \simeq 17$ GHz (all other parameters defined above), we have that $x_{ZPF}/\xi \simeq 3 \cdot 10^{-3}$, $g_2 \simeq 40$ kHz.

Also, note that the Hamiltonian given in Eq. (5) is valid in the case of equal JJs. If the JJs exhibit some degree of asymmetry, a linear coupling to σ_z and a quadratic coupling to σ_x appear, in addition to a small qubit rotation (zeroth-order term in σ_x). While the quadratic coupling to σ_x is negligible for all parameters, the linear coupling between the displacement and σ_z becomes comparable to the quadratic one when the asymmetry of the Josephson energies is $\sim \frac{x_{ZPF}}{2\xi}$, which, for the parameters chosen here, corresponds to

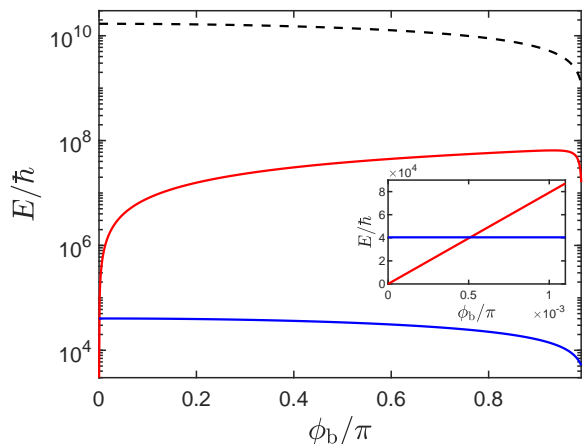


FIG. 2. The strengths of g_1 (red) and g_2 (blue) couplings and the qubit frequency ω_q (dashed black) as a function of the external flux ϕ_b . The inset shows the crossover point near zero flux bias where g_1 becomes larger than g_2 . Parameters $E_J = 20$ GHz, $E_C = 1$ GHz, $x_{ZPF}/\xi = 3 \cdot 10^{-3}$.

$\Delta E_J = |E_{J1} - E_{J2}| \simeq 30$ MHz. Furthermore, the zeroth-order term in σ_x is negligible whenever the asymmetry $d_0 = |E_{J1} - E_{J2}| / |E_{J1} + E_{J2}|$ is (much) less than unity. A discussion of the general case of different JJs is presented in the Supplemental Material.

III. STATE SWAPPING PROTOCOL

A promising application for the setup proposed here is bosonic error correction. On general grounds, bosonic error correction provides key advantages over quantum error correction schemes utilizing multiple physical qubits, inasmuch it eliminates the overheads and the potential issues arising from cross-talk of multiple physical

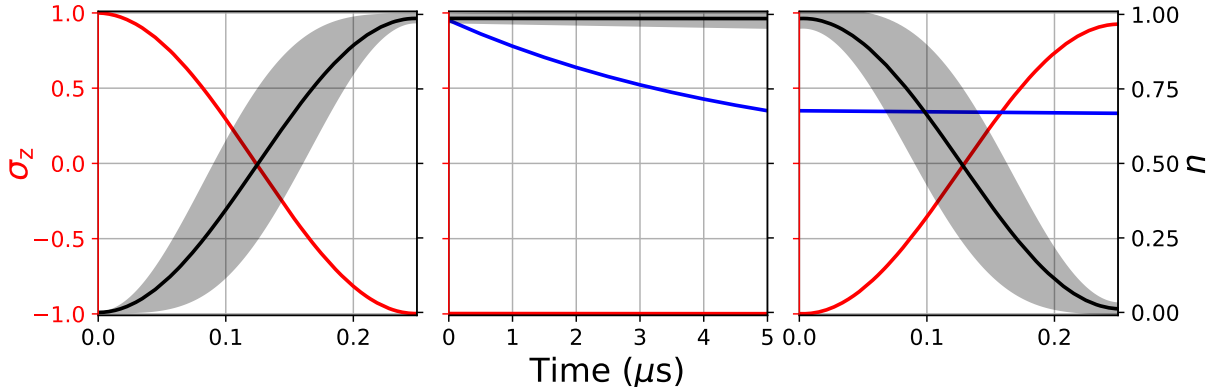


FIG. 3. Demonstration of the state swapping protocol. *Left panel:* the qubit state $|\sigma_z = 1\rangle$ (red line) is transferred to the mechanical oscillator Fock state $|n = 1\rangle$ (black line/black shade). *Central panel:* the linear coupling g_1 is suppressed. The free evolution of the state $|n = 1\rangle$ is subject to the (small) intrinsic dissipation of the mechanical resonator. *Right panel:* the state $|n = 1\rangle$ is transferred back to the qubit. The fidelity of the swapping to the mechanical resonator and back, is compared with the free evolution of the $|\sigma_z = 1\rangle$ state under subject to pure qubit decoherence (blue line). Parameters: $E_C = 1$ GHz, $E_J = 20$ GHz, $x_{ZPF}/\xi = 3 \cdot 10^{-3}$, $\phi_{b,0} = 0.5$, mechanical angular frequency $\omega_m = 1$ GHz and damping rate $\gamma = 1$ kHz, qubit damping rate $\gamma_\sigma = 100$ kHz. In the simulations, we have assumed a finite temperature of 10 mK, both for the qubit and for the mechanical bath, corresponding to a population of $n_{\sigma,th} \simeq 2 \cdot 10^{-7}$ and $n_{m,th} \simeq 0.87$, respectively. The time axis is reset to zero for each step in the protocol to better illustrate the different time scales.

qubits. More specifically, our mechanical implementation has further advantages over a microwave cavity: mechanical resonators offer better ringdown times than microwave cavities, shuttling resonators offer a more compact design and relatively straightforward scalability, and the qubit/mechanics (linear) coupling can be externally tuned.

As a first step in this direction, we consider a state-swapping protocol that demonstrates the ability of this device to coherently transfer a qubit state to a quantum state of the mechanical resonator. Given the relatively large frequency mismatch between the qubit and the mechanics ($\omega_q/\omega_m \simeq 20$), direct transitions between mechanics and qubit are highly non-resonant. To induce such sideband transitions, we therefore modulate the flux through the JJs loop at a frequency $\bar{\omega}$, corresponding to a phase modulation given by $\phi_b(t) = \phi_{b,0} \cos(\bar{\omega}t)$ (flux-driven sideband transitions). This technique is analogous to the one employed in Ref. [43] for the case of a transmon qubit coupled to a microwave cavity. In the context of optomechanical systems, a similar approach was also considered in [30], where the gate charge modulation was used to induce single-phonon transitions in a mechanical resonator coupled to a qubit. In general, these techniques go under the name of ac-dither techniques [44].

As a consequence of the phase modulation, the coefficients appearing in the definition of the Hamiltonian H in Eq. (5) become time dependent.

$$H = \frac{\omega_q(t)}{2} \sigma_z + \omega_m(t) b^\dagger b + g_1(t) (b^\dagger + b) \sigma_x + g_2(t) (b^\dagger + b)^2 \sigma_z. \quad (6)$$

It is possible to show that, in a non-uniformly ro-

tating frame for the qubit and the mechanics, if the driving frequency is chosen in such a way that $\bar{\omega} = \bar{\omega}_q - \omega_m$, with $\bar{\omega}_q = \omega_q|_{\phi_b=0} - \delta_q$, $\delta_q = \phi_{b0}^2 \omega_{p0}/16$ and $\omega_{p0} = \sqrt{16 E_C E_J \cos(\phi_b/2)}$ for symmetrical JJs, the transformed Hamiltonian corresponds to a state-swapping Hamiltonian

$$H' = g_{sw} (b^\dagger \sigma_- + b \sigma_+) \quad (7)$$

where $g_{sw} = \bar{g}_1 J_0(\delta_q/2\bar{\omega})$ with $J_0(x)$ being the 0th-order Bessel function and \bar{g}_1 the linear approximation of $g_1(t)$ with respect to $\phi_{b,0}$.

Given that $\phi_{b,0}$ is externally tunable, after the state-swapping transition described above, it is possible to externally suppress the linear coupling between the qubit and the mechanical resonator. Having this in mind, one can consider using the mechanical mode as a low-decoherence memory element, owing to the combined effect of the on-demand suppression of lowest-order coupling between the qubit and the mechanical resonator, and the intrinsically long decoherence times of the mechanical element.

In Fig. 3, we depict a simple instance of the state-swapping protocol. Starting from the state $|\sigma_z = 1, n_m = 0\rangle$, we first perform a state swap between the qubit state and the mechanics (left), followed by the “free” evolution in the absence of qubit-mechanics coupling – $\phi_b = 0$, implying $g_1 = 0$ – (center), transferring then the excitation back to the qubit (right). We have compared this state-swapping protocol with the free evolution of the $|\sigma_z = 1\rangle$ state in the presence of the same environment (qubit decay rate $\gamma_\sigma = 100$ kHz) as for the state-swap protocol. The $|\sigma_z = 1, n_m = 0\rangle$ initial state can be prepared resorting to a preliminary cooling step of the mechanical mode.

We would like to point out that, while the parameters chosen here push the boundaries of what is experimentally realizable, with values of the $f \cdot Q$ product of the order of 10^{14} , record values of $f \cdot Q = O(10^{18})$ have been reported for bulk acoustic wave resonators [45, 46].

IV. EXPERIMENTAL OUTLOOK AND PERFORMANCE

From an experimental point of view, the realization of a shuttling island (orange box in Fig. 1) can be performed with some additional processing steps. However, fabrication of a superconducting island has turned out to be a challenge so far, since standard superconducting materials, such as Al, tend to oxidize through for small 50^3nm^3 islands. Our latest work on that end shows that we can realize superconducting NbN-strips [47] with a $T_c = 9\text{K}$, which avoids the aforementioned issue and is fully compatible with our processing techniques. Hence, the fabrication of superconducting islands in varying circuit combinations is possible now. One of the circuits to be implemented is shown in Fig. 1.

Additionally, the ability to perform precise ac-dither protocols with the magnetic flux is required to successfully operate the device as a platform for useful quantum operations. These techniques are, in principle, possible with tuning either the gate charge or the magnetic flux [44], and different kinds of modulation schemes have been experimentally demonstrated to be feasible, e.g. Ref.[30] for charge-based and Refs. [43, 48] for flux-based procedures.

Note that, in this work, we do not focus on parameter optimization for our device, for example, to maximize the couplings or to minimize the noise in the circuit, but instead we use fairly typical values for superconducting circuits. As an example, one could introduce a larger shunting capacitance to avoid charge noise effects thanks to the reduced charging energy, placing the device firmly in the $E_J \gg E_C$ transmon regime.

Even though we are not aiming to optimize the performance of our device here, the accessible coupling strengths between the qubit and the mechanics are promising when considering the proposed device as a candidate for practical quantum computation protocols. We obtain a quadratic coupling g_2 that is about an order of magnitude larger than presently achievable linewidths for shuttling mechanical resonators using the parameters in Fig. 2 for a wide range of flux biasing, and $g_2/\omega_m \approx$

4×10^{-5} which is comparable to different state-of-the-art implementations of bosonic error correction schemes. For example, in a recent demonstration of quantum error correction beyond the break-even point using a bosonic (photonic) GKP code [38], the corresponding ratio was $\sim 1 \times 10^{-5}$ with a superconducting cavity as the bosonic system. However, we do not predict reaching the ultra-strong coupling limit as in Ref. [30], but in terms of the linear coupling g_1 , we still can attain significantly larger values than the resonator linewidth with $g_1/\omega_m > 0.01$ already starting from a small flux bias.

We want to emphasize that the state swapping protocol explored in this work is not meant to be a comprehensive procedure for bosonic error correction, but instead a proof of concept that our device could be useful in such applications. Indeed, it is possible to create arbitrary phonon number states with detailed control of the state swapping Hamiltonian [49] and, additionally, other interesting and useful operations can be realized with this interaction alone, such as the preparation of a mechanical cat states [11]. On top of this linear interaction between the qubit and the mechanics, we also have access to another resource, namely the quadratic coupling, that is largely unexplored in this work.

V. CONCLUSIONS

In our work, we introduce a novel device (the X2MON) which consists of a transmon coupled to a mechanical shuttle operating in the quantum regime. We discuss the nature of the coupling between the two. Furthermore, we demonstrate a state-swap protocol, which, owing to the properties of the shuttle, can be directly employed as a quantum memory. Our work paves the way for bosonic error correction with mechanical modes.

ACKNOWLEDGMENTS

The numerical simulations were performed using the `QuantumOptics.jl` numerical framework [50]. FM and JM acknowledge financial support from the Research Council of Norway (Grant No. 333937) through participation in the QuantERA ERA-NET Cofund in Quantum Technologies. RHB acknowledges collaboration with Nexperia GmbH, Germany.

[1] W. Marshall, C. Simon, R. Penrose, and D. Bouwmeester, Towards Quantum Superpositions of a Mirror, *Physical Review Letters* **91**, 130401 (2003).
 [2] M. Aspelmeyer, T. J. Kippenberg, and F. Marquardt, Cavity optomechanics, *Reviews of Modern Physics* **86**, 1391 (2014).

[3] S. Barzanjeh, A. Xuereb, S. Gröblacher, M. Paternostro, C. A. Regal, and E. M. Weig, Optomechanics for quantum technologies, *Nature Physics* **18**, 15 (2022).
 [4] J. D. Teufel, T. Donner, D. Li, J. W. Harlow, M. S. Allman, K. Cicak, A. J. Sirois, J. D. Whittaker, K. W. Lehnert, and R. W. Simmonds, Sideband cooling of mi-

- chromechanical motion to the quantum ground state, *Nature* **475**, 359 (2011).
- [5] M. Rossi, D. Mason, J. Chen, Y. Tsaturyan, and A. Schliesser, Measurement-based quantum control of mechanical motion, *Nature* **563**, 53 (2018).
- [6] E. E. Wollman, C. U. Lei, A. J. Weinstein, J. Suh, A. Kronwald, F. Marquardt, A. A. Clerk, and K. C. Schwab, Quantum squeezing of motion in a mechanical resonator., *Science* **349**, 952 (2015).
- [7] J. M. Pirkkalainen, E. Damskäg, M. Brandt, F. Massel, and M. A. Sillanpää, Squeezing of Quantum Noise of Motion in a Micromechanical Resonator, *Physical Review Letters* **115**, 243601 (2015).
- [8] R. Riedinger, A. Wallucks, I. Marinkovic, C. Löschnauer, M. Aspelmeyer, S. Hong, and S. Gröblacher, Remote quantum entanglement between two micromechanical oscillators, *Nature* **556**, 473 (2018).
- [9] C. F. Ockeloen-Korppi, E. Damskäg, J. M. Pirkkalainen, M. Asjad, A. A. Clerk, F. Massel, M. J. Woolley, and M. A. Sillanpää, Stabilized entanglement of massive mechanical oscillators, *Nature* **556**, 478 (2018).
- [10] Y. Chu, P. Kharel, T. Yoon, L. Frunzio, P. T. Rakich, and R. J. Schoelkopf, Creation and control of multi-phonon Fock states in a bulk acoustic-wave resonator, *Nature* **563**, 666 (2018).
- [11] M. Bild, M. Fadel, Y. Yang, U. v. Lüpke, P. Martin, A. Bruno, and Y. Chu, Schrödinger cat states of a 16-microgram mechanical oscillator, *Science* **380**, 274 (2023).
- [12] T. T. Heikkilä, F. Massel, J. Tuorila, R. Khan, and M. A. Sillanpää, Enhancing Optomechanical Coupling via the Josephson Effect, *Physical Review Letters* **112**, 203603 (2014).
- [13] P. D. Nation, J. Suh, and M. P. Blencowe, Ultrastrong optomechanics incorporating the dynamical Casimir effect, *Physical Review A* **93**, 022510 (2016).
- [14] E. Romero-Sánchez, W. P. Bowen, M. R. Vanner, K. Xia, and J. Twamley, Quantum magnetomechanics: Towards the ultrastrong coupling regime, *Physical Review B* **97**, 024109 (2018).
- [15] L. Neumeier, T. E. Northup, and D. E. Chang, Reaching the optomechanical strong-coupling regime with a single atom in a cavity, *Physical Review A* **97**, 063857 (2018).
- [16] L. Neumeier and D. E. Chang, Exploring unresolved sideband, optomechanical strong coupling using a single atom coupled to a cavity, *New Journal of Physics* **20**, 083004 (2018).
- [17] A. Settineri, V. Macrì, A. Ridolfo, O. D. Stefano, A. F. Kockum, F. Nori, and S. Savasta, Dissipation and thermal noise in hybrid quantum systems in the ultrastrong-coupling regime, *Physical Review A* **98**, 053834 (2018).
- [18] M. Kounalakis, Y. M. Blanter, and G. A. Steele, Flux-mediated optomechanics with a transmon qubit in the single-photon ultrastrong-coupling regime, *Physical Review Research* **2**, 023335 (2020).
- [19] J.-Q. Liao, J.-F. Huang, L. Tian, L.-M. Kuang, and C.-P. Sun, Generalized ultrastrong optomechanical-like coupling, *Physical Review A* **101**, 063802 (2020).
- [20] J. Manninen, M. T. Haque, D. Vitali, and P. Hakonen, Enhancement of the optomechanical coupling and Kerr nonlinearity using the Josephson capacitance of a Cooper-pair box, *Physical Review B* **105**, 144508 (2022).
- [21] J. M. Pirkkalainen, S. U. Cho, F. Massel, J. Tuorila, T. T. Heikkilä, P. J. Hakonen, and M. A. Sillanpää, Cavity optomechanics mediated by a quantum two-level system, *Nature communications* **6**, 6981 (2015).
- [22] T. Bera, S. Majumder, S. K. Sahu, and V. Singh, Large flux-mediated coupling in hybrid electromechanical system with a transmon qubit, *Communications Physics* **4**, 12 (2021).
- [23] J. D. Thompson, B. M. Zwickl, A. M. Jayich, F. Marquardt, S. M. Girvin, and J. G. E. Harris, Strong dispersive coupling of a high-finesse cavity to a micromechanical membrane, *Nature* **452**, 72 (2008).
- [24] A. M. Jayich, J. C. Sankey, B. M. Zwickl, C. Yang, J. D. Thompson, S. M. Girvin, A. A. Clerk, F. Marquardt, and J. G. E. Harris, Dispersive optomechanics: A membrane inside a cavity, *New Journal Of Physics* **10**, 095008 (2008).
- [25] F. Helmer, M. Mariani, E. Solano, and F. Marquardt, Quantum nondemolition photon detection in circuit QED and the quantum Zeno effect, *Physical Review A* **79**, 052115 (2009).
- [26] H. Miao, S. Danilishin, T. Corbitt, and Y. Chen, Standard Quantum Limit for Probing Mechanical Energy Quantization, *Physical Review Letters* **103**, 100402 (2009).
- [27] A. Nunnenkamp, K. Børkje, J. G. E. Harris, and S. M. Girvin, Cooling and squeezing via quadratic optomechanical coupling, *Physical Review A* **82**, 021806 (2010).
- [28] T. P. Purdy, D. W. C. Brooks, T. Botter, N. Brahms, Z.-Y. Ma, and D. M. Stamper-Kurn, Tunable cavity optomechanics with ultracold atoms, *Physical Review Letters* **105**, 133602 (2010).
- [29] J. J. Viennot, X. Ma, and K. W. Lehnert, Phonon-Number-Sensitive Electromechanics., *Physical Review Letters* **121**, 183601 (2018).
- [30] X. Ma, J. J. Viennot, S. Kotler, J. D. Teufel, and K. W. Lehnert, Non-classical energy squeezing of a macroscopic mechanical oscillator, *Nature Physics* **17**, 322 (2021).
- [31] D. V. Scheible and R. H. Blick, Silicon nanopillars for mechanical single-electron transport, *Applied Physics Letters* **84**, 4632 (2004).
- [32] D. R. Koenig, E. M. Weig, and J. P. Kotthaus, Ultrasonically driven nanomechanical single-electron shuttle, *Nature Nanotechnology* **3**, 482 (2008).
- [33] C. Kim, M. Prada, and R. H. Blick, Coulomb blockade in a coupled nanomechanical electron shuttle, *ACS Nano* **6**, 651 (2012).
- [34] L. Y. Gorelik, A. Isacsson, Y. M. Galperin, R. I. Shekhter, and M. Jonson, Coherent transfer of Cooper pairs by a movable grain, *Nature* **411**, 454 (2001).
- [35] C. Kim, R. Marsland, and R. H. Blick, The nanomechanical bit, *Small* **16**, 2001580 (2020).
- [36] J. Koch, T. M. Yu, J. Gambetta, A. A. Houck, D. I. Schuster, J. Majer, A. Blais, M. H. Devoret, S. M. Girvin, and R. J. Schoelkopf, Charge-insensitive qubit design derived from the Cooper pair box, *Physical Review A* **76**, 042319 (2007).
- [37] M. H. Michael, M. Silveri, R. T. Brierley, V. V. Albert, J. Salmilehto, L. Jiang, and S. M. Girvin, New class of quantum error-correcting codes for a bosonic mode, *Physical Review X* **6**, 031006 (2016).
- [38] V. V. Sivak, A. Eickbusch, B. Royer, S. Singh, I. Tsioutsios, S. Ganjam, A. Miano, B. L. Brock, A. Z. Ding, L. Frunzio, S. M. Girvin, R. J. Schoelkopf, and M. H. De-

- voret, Real-time quantum error correction beyond break-even, *Nature* **616**, 50 (2023).
- [39] V. Ambegaokar and A. Baratoff, Tunneling Between Superconductors, *Physical Review Letters* **10**, 486 (1963).
- [40] J. M. Martinis, Course 13 Superconducting qubits and the physics of Josephson junctions, *Les Houches* **79**, 487 (2004).
- [41] R. Landauer, Spatial Variation of Currents and Fields Due to Localized Scatterers in Metallic Conduction, *IBM Journal of Research and Development* **1**, 223 (1957).
- [42] S. M. Girvin, Superconducting qubits and circuits: Artificial atoms coupled to microwave photons, *École d'été Les Houches* (2011).
- [43] J. D. Strand, M. Ware, F. Beaudoin, T. A. Ohki, B. R. Johnson, A. Blais, and B. L. T. Plourde, First-order sideband transitions with flux-driven asymmetric transmon qubits, *Physical Review B* **87**, 220505 (2013).
- [44] A. Blais, J. Gambetta, A. Wallraff, D. I. Schuster, S. M. Girvin, M. H. Devoret, and R. J. Schoelkopf, Quantum-information processing with circuit quantum electrodynamics, *Physical Review A* **75**, 032329 (2007).
- [45] S. Galliou, M. Goryachev, R. Bourquin, P. Abbé, J. P. Aubry, and M. E. Tobar, Extremely Low Loss Phonon-
Trapping Cryogenic Acoustic Cavities for Future Physical Experiments, *Scientific Reports* **3**, 2132 (2013).
- [46] P. Kharel, Y. Chu, M. Power, W. H. Renninger, R. J. Schoelkopf, and P. T. Rakich, Ultra-high-Q phononic resonators on-chip at cryogenic temperatures, *APL Photonics* **3**, 066101 (2018).
- [47] I. González Díaz-Palacio, M. Wenskat, G. K. Deyu, W. Hillert, R. H. Blick, and R. Zierold, Thermal annealing of superconducting niobium titanium nitride thin films deposited by plasma-enhanced atomic layer deposition, *Journal of Applied Physics* **134**, 035301 (2023).
- [48] J. A. Valery, S. Chowdhury, G. Jones, and N. Didier, Dynamical sweet spot engineering via two-tone flux modulation of superconducting qubits, *PRX Quantum* **3**, 020337 (2022).
- [49] C. K. Law and J. H. Eberly, Arbitrary control of a quantum electromagnetic field, *Physical Review Letters* **76**, 1055 (1996).
- [50] S. Krämer, D. Plankensteiner, L. Ostermann, and H. Ritsch, *QuantumOptics.jl*: A Julia framework for simulating open quantum systems, *Computer Physics Communications* **227**, 109 (2018).

**Hybrid optomechanical superconducting qubit system –
SUPPLEMENTAL MATERIAL**

Juuso Manninen,¹ Robert H. Blick,^{2,3} and Francesco Massel^{1,*}

¹*Department of Science and Industry Systems,
University of South-Eastern Norway, PO Box 235, Kongsberg, Norway*

²*Center for Hybrid Nanostructures (CHyN), Universität Hamburg,
Luruper Chaussee 149, Hamburg 22761 Germany*

³*Materials Science and Engineering, University of Wisconsin-Madison,
1509 University Ave. WI 53706 U.S.A.*

arXiv:2402.18317v1 [quant-ph] 28 Feb 2024

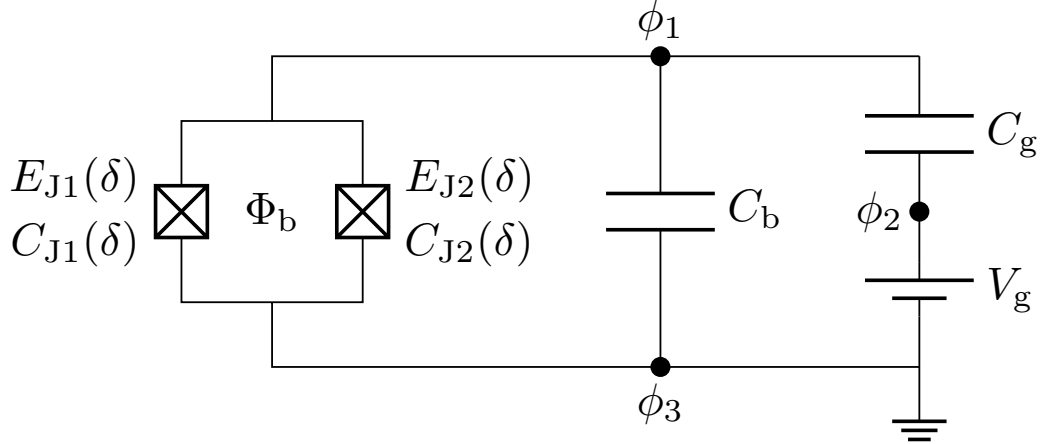


FIG. 1. Schematic of the SUNMESH circuit. For the formal calculation, the voltage source is replaced by a capacitor C_{V_g} allowing voltage V_g to be induced on island 2.

DERIVATION OF THE X2MON HAMILTONIAN

We present here a full derivation of the Hamiltonian of the X2MON circuit (see Fig. 1) and of the couplings between the mechanical motion and the qubit that arise in the system. The calculation here generalizes the discussion of the main text, we do not assume the Josephson junctions in the system to be symmetric. Note that we use the convention $\hbar = 1$.

Lumped-element description

We derive the Hamiltonian for the X2MON circuit with standard circuit quantum electrodynamics (circuit-QED) methods [1, 2]. The flux at the node i at time t is given by

$$\Phi_i(t) = \int^t V_i(\tau) d\tau, \quad (\text{SI1})$$

which defines the voltage of the node as

$$V_i(t) = \dot{\Phi}_i. \quad (\text{SI2})$$

The node flux and phase are connected with the following relation

$$\phi_i = 2\pi \frac{\Phi_i}{\Phi_0}, \quad (\text{SI3})$$

where $\Phi_0 = \frac{h}{2e}$ is the flux quantum. The indices of different nodes in our circuit are given in Fig. 1.

The energy related to the capacitive elements of the circuit is given by

$$\mathcal{T} = \frac{C_{J1} + C_{J2} + C_b}{2} \dot{\Phi}_1^2 + \frac{C_g}{2} (\dot{\Phi}_1 - \dot{\Phi}_2)^2 + \frac{C_{V_g}}{2} \dot{\Phi}_2^2. \quad (\text{SI4})$$

Here C_{J1} and C_{J2} are the capacitances of the Josephson junctions, C_g is the gate capacitance, and C_b the shunting capacitance that is large so that our qubit operates in the TRANS-MON regime. C_{V_g} is an additional capacitance, replacing the voltage source for the formal calculation, whose only function in this formalism is to induce the voltage bias on the qubit island, see Ref. [1]. Note that $\dot{\Phi}_3$ is not present here, since $\dot{\Phi}_3 = 0$ is due to that node being grounded. Only the Josephson junctions contribute to the inductive energy of the circuit,

$$\begin{aligned} \mathcal{U} &= -E_{J1}(\delta) \cos\left(2\pi \frac{\Phi_1 + \frac{1}{2}\Phi_b}{\Phi_0}\right) - E_{J2}(\delta) \cos\left(2\pi \frac{\Phi_1 - \frac{1}{2}\Phi_b}{\Phi_0}\right) \\ &= -(E_{J1}(\delta) + E_{J2}(\delta)) \left(\cos\phi_1 \cos\frac{\phi_b}{2} + d(\delta) \sin\phi_1 \sin\frac{\phi_b}{2} \right), \end{aligned} \quad (\text{SI5})$$

where $d(\delta) = (E_{J2}(\delta) - E_{J1}(\delta))/(E_{J1}(\delta) + E_{J2}(\delta))$ and the Josephson energies are given by

$$E_{J1}(\delta) = \tilde{E}_{J10} e^{-\frac{x_0 + \delta}{\xi}} = E_{J1} e^{-\frac{\delta}{\xi}}, \quad (\text{SI6a})$$

$$E_{J2}(\delta) = \tilde{E}_{J20} e^{-\frac{x_0 - \delta}{\xi}} = E_{J2} e^{\frac{\delta}{\xi}}. \quad (\text{SI6b})$$

Anticipating our analysis of the device dynamics, in Eqs. (SI5,SI6), we have explicitly indicated the JJ energy dependence on the deviation (δ) from the equilibrium position(x_0) of the shuttle.

Josephson energy

We provide here a brief explanation of the forms of the Josephson energies of the two junctions given in Eq. (SI6). Let us assume that the normal state resistance of the junctions is

$$R_N = R_{N0} \exp\left[\frac{x}{\xi}\right], \quad (\text{SI7})$$

stemming from the exponentially suppressed tunneling probability across the junction as a function of its thickness x . The Ambegaokar–Baratoff formula [3, 4] provides the following expression for the JJ energy

$$E_J(\phi) = -\frac{1}{8} \frac{R_K}{R_N} \Delta \cos\phi, \quad (\text{SI8})$$

where $R_K = \frac{2\pi\hbar}{e^2}$ is the resistance quantum, Δ the superconducting gap, and ϕ the superconducting phase difference across the junction. Focusing on the characteristic Josephson energy $E_J = |E_J(\phi = 0)|$, we get Eq. (SI6) with the help of the Landauer formula [5] and Eq. (SI7), where the parameter ξ is given by

$$\xi = \frac{x_0}{\log \left[\frac{\Delta}{8E_J} \frac{R_K}{R_{N0}} \right]}. \quad (\text{SI9})$$

X2MON Hamiltonian

The Lagrangian of the system, including the Lagrangian of the shuttle $\mathcal{L}_m(x_m, p_m)$,

$$\mathcal{L} = \mathcal{T} - \mathcal{U} = \frac{1}{2} \vec{\Phi}^\top [C] \vec{\Phi} - \mathcal{U} + \mathcal{L}_m(x_m, p_m) \quad (\text{SI10})$$

can be written using the capacitance matrix

$$[C] = \begin{pmatrix} C_{J1} + C_{J2} + C_b + C_g & -C_g \\ -C_g & C_g + C_{V_g} \end{pmatrix} \quad (\text{SI11})$$

whose inverse is

$$[C]^{-1} = \frac{1}{(C_g + C_b)(C_g + C_{V_g}) + C_g C_{V_g}} \begin{pmatrix} C_g + C_{V_g} & C_g \\ C_g & C_g + C_b + C_g \end{pmatrix} = \begin{pmatrix} \frac{1}{C_{11}} & \frac{1}{C_{12}} \\ \frac{1}{C_{12}} & \frac{1}{C_{22}} \end{pmatrix}. \quad (\text{SI12})$$

The Hamiltonian can be expressed using this inverse capacitance matrix

$$\begin{aligned} \mathcal{H} &= \sum_i \dot{\Phi}_i \frac{\partial \mathcal{L}}{\partial \dot{\Phi}_i} + \dot{x}_m \frac{\partial \mathcal{L}}{\partial \dot{x}_m} - \mathcal{L} \\ &= \sum_i \dot{\Phi}_i Q_i + \dot{x}_m \frac{\partial \mathcal{L}}{\partial \dot{x}_m} - \mathcal{L} \\ &= \frac{1}{2} \vec{Q}^\top [C]^{-1} \vec{Q} + \mathcal{U} + E(x_m, p_m) \\ &= \frac{1}{2C_{11}} Q_1^2 + \frac{1}{C_{12}} Q_1 Q_2 + \frac{1}{2C_{22}} Q_2^2 + \mathcal{U} + E(x_m, p_m), \end{aligned} \quad (\text{SI13})$$

where $E(x_m, p_m)$ is the (elastic) energy of the shuttle, and the conjugate variable to flux Φ_i are charges on each island $Q_i = \frac{\partial \mathcal{L}}{\partial \dot{\Phi}_i}$. Note that the voltage on island 2, $\frac{\partial \mathcal{H}}{\partial Q_2}$, can now be set to the gate voltage V_g by choosing $V_g = \frac{Q_2}{C_{22}}$ and letting $C_{V_g} \rightarrow \infty$.

Now, defining the number of Cooper pairs on the qubit island, the charging energy of the qubit, and the gate charge

$$\begin{aligned} n &= \frac{Q_1}{2e}, \\ E_C(\delta) &= \frac{e^2}{2C_{11}} \xrightarrow{C_{V_g} \rightarrow \infty} \frac{e^2}{2(C_{J1}(\delta) + C_{J2}(\delta) + C_b + C_g)}, \\ n_g &= -\frac{1}{2e} \frac{C_{11}C_{22}}{C_{12}} V_g \xrightarrow{C_{V_g} \rightarrow \infty} -\frac{C_g}{2e} V_g, \end{aligned} \quad (\text{SI14})$$

the Hamiltonian in Eq. (SI13) can be written in the canonical form

$$\mathcal{H} = 4E_C(\delta)(n - n_g)^2 + \mathcal{U} + E(x_m, p_m) + 2e^2 n_g^2 \left(\frac{C_{12}^2}{C_{11}^2 C_{22}} - \frac{1}{C_{11}} \right), \quad (\text{SI15})$$

where the last term can be ignored due to it providing only a constant contribution to the total energy of the system and not affecting its dynamics.

Quantization of the Hamiltonian

Firstly, we expand the potential energy part of the Hamiltonian in Eq. (SI15) up to the fourth order in ϕ_1

$$\begin{aligned} \mathcal{H} &\approx 4E_C(\delta)(n - n_g)^2 + E(x_m, p_m) \\ &\quad - (E_{J1}(\delta) + E_{J2}(\delta)) \cos \frac{\phi_b}{2} \left(1 - \frac{\phi_1^2}{2} + \frac{\phi_1^4}{24} \right) \\ &\quad - (E_{J1}(\delta) + E_{J2}(\delta)) d(\delta) \sin \frac{\phi_b}{2} \left(\phi_1 - \frac{\phi_1^3}{6} \right). \end{aligned} \quad (\text{SI16})$$

We then promote the phase ϕ and n to quantum operators $\hat{\phi}$ and \hat{n} , respectively. These obey canonical commutation relations

$$\left[\hat{\phi}_1, \hat{n} \right] = i, \quad (\text{SI17})$$

We can express them in terms of bosonic lowering (raising) operators a (a^\dagger), which obey the standard bosonic commutation relation $[a, a^\dagger] = 1$, as

$$\hat{\phi}_1 = \phi_{\text{ZPF}}(a^\dagger + a), \quad (\text{SI18a})$$

$$\hat{n} = in_{\text{ZPF}}(a^\dagger - a). \quad (\text{SI18b})$$

Substituting these definitions into Eq. (SI17) implies for the zero-point fluctuations

$$\phi_{\text{ZPF}} n_{\text{ZPF}} = \frac{1}{2}. \quad (\text{SI19})$$

The quantized form of the Hamiltonian, Eq. (SI16), can then be written as

$$\begin{aligned}
\hat{H} = & \left(4E_C(\delta)n_{\text{ZPF}}^2 + \frac{1}{2}(E_{\text{J1}}(\delta) + E_{\text{J2}}(\delta)) \cos \frac{\phi_b}{2} \phi_{\text{ZPF}}^2 \right) (2a^\dagger a + 1) \\
& + \left(-4E_C(\delta)n_{\text{ZPF}}^2 + \frac{1}{2}(E_{\text{J1}}(\delta) + E_{\text{J2}}(\delta)) \cos \frac{\phi_b}{2} \phi_{\text{ZPF}}^2 \right) (a^{\dagger 2} + a^2) \\
& - (E_{\text{J1}}(\delta) + E_{\text{J2}}(\delta)) \cos \frac{\phi_b}{2} \left(1 + \frac{\hat{\phi}^4}{24} \right) \\
& - (E_{\text{J1}}(\delta) + E_{\text{J2}}(\delta)) d(\delta) \sin \frac{\phi_b}{2} \left(\hat{\phi} - \frac{\hat{\phi}^3}{6} \right) \\
& + E(x_0 + \delta, p_m).
\end{aligned} \tag{SI20}$$

Within the conventional harmonic description [1], recalling the identity Eq. (SI19), we can express the zero-point fluctuations as

$$\begin{aligned}
n_{\text{ZPF}}(\delta) &= \left\{ \frac{E_{\text{J1}}(\delta) + E_{\text{J2}}(\delta)}{32E_C(\delta)} \cos \frac{\phi_b}{2} \right\}^{\frac{1}{4}}, \\
\phi_{\text{ZPF}}(\delta) &= \left\{ \frac{2E_C(\delta)}{(E_{\text{J1}}(\delta) + E_{\text{J2}}(\delta)) \cos \frac{\phi_b}{2}} \right\}^{\frac{1}{4}},
\end{aligned} \tag{SI21}$$

and the full expression of the Hamiltonian becomes

$$\begin{aligned}
\hat{H} = & \omega_p(\delta)(a^\dagger a + \frac{1}{2}) + E(x_0 + \delta, p_m) \\
& - (E_{\text{J1}}(\delta) + E_{\text{J2}}(\delta)) \cos \frac{\phi_b}{2} - \frac{1}{12}E_C(\delta)(a^\dagger + a)^4 \\
& - (E_{\text{J1}}(\delta) + E_{\text{J2}}(\delta)) d(\delta) \sin \frac{\phi_b}{2} \phi_{\text{ZPF}}(\delta)(a^\dagger + a) \\
& + \frac{1}{6}(E_{\text{J1}}(\delta) + E_{\text{J2}}(\delta)) d(\delta) \sin \frac{\phi_b}{2} \phi_{\text{ZPF}}^3(\delta)(a^\dagger + a)^3,
\end{aligned} \tag{SI22}$$

where

$$\omega_p(\delta) = \sqrt{8E_C(\delta)(E_{\text{J1}}(\delta) + E_{\text{J2}}(\delta)) \cos \frac{\phi_b}{2}}. \tag{SI23}$$

DERIVING THE COUPLING BETWEEN THE QUBIT AND THE MECHANICS

We now expand the Hamiltonian in Eq. (SI22) with respect to the mechanical displacement up to the second order and denote the quantized mechanical displacement (obeying canonical commutation relations) with $\hat{\delta} = x_{\text{ZPF}}(b^\dagger + b)$. The following shorthand notation is used to display the results in a more compact form: $E_C = E_C(0)$, $E_{\text{J1}} = E_{\text{J1}}(0)$,

$E_{J2} = E_{J2}(0)$, and $d_0 = d(0)$. The Josephson capacitances are approximated with parallel-plate capacitors, i.e. the charging energy has the form

$$E_C(\delta) = \frac{e^2}{2 \left(\frac{C_J}{1+\frac{\delta}{x_0}} + \frac{C_J}{1-\frac{\delta}{x_0}} + C_b + C_g \right)}, \quad (\text{SI24})$$

where $C_J = C_{J1}(0) = C_{J2}(0)$.

Let us go through the expansion of the Hamiltonian, Eq. (SI22), term by term. The coefficient definitions are summarized below in Eq. (SI33) for the reader's convenience.

For the $(a^\dagger a + \frac{1}{2})$ term, we obtain

$$\begin{aligned} & \omega_p(\hat{\delta})(a^\dagger a + \frac{1}{2}) \\ & \approx \left\{ \sqrt{8E_C(E_{J1} + E_{J2}) \cos \frac{\phi_b}{2}} + d_0 \sqrt{2E_C(E_{J1} + E_{J2}) \cos \frac{\phi_b}{2} \frac{x_{\text{ZPF}}}{\xi}} (b^\dagger + b) \right. \\ & \quad \left. + \sqrt{8E_C(E_{J1} + E_{J2}) \cos \frac{\phi_b}{2}} \left[\frac{1}{2\xi^2} - \frac{2C_J}{(2C_J + C_b + C_g)x_0^2} - \frac{d_0^2}{4\xi^2} \right] x_{\text{ZPF}}^2 (b^\dagger + b)^2 \right\} \\ & \quad \times (a^\dagger a + \frac{1}{2}) \quad (\text{SI25}) \\ & \approx \left\{ \sqrt{8E_C(E_{J1} + E_{J2}) \cos \frac{\phi_b}{2}} + d_0 \sqrt{2E_C(E_{J1} + E_{J2}) \cos \frac{\phi_b}{2} \frac{x_{\text{ZPF}}}{\xi}} (b^\dagger + b) \right. \\ & \quad \left. + \frac{1}{2} \sqrt{2E_C(E_{J1} + E_{J2}) \cos \frac{\phi_b}{2}} \left(\frac{x_{\text{ZPF}}}{\xi} \right)^2 (b^\dagger + b)^2 \right\} (a^\dagger a + \frac{1}{2}) \\ & = \{ \omega_{p0} + g_{21}(b^\dagger + b) + g_{22}(b^\dagger + b)^2 \} (a^\dagger a + \frac{1}{2}), \end{aligned}$$

and the term related to $(a^\dagger + a)^4$ gives

$$\begin{aligned} -\frac{E_C(\hat{\delta})}{12}(a^\dagger + a)^4 & \approx \left\{ -\frac{E_C}{12} + \frac{1}{3e^2} E_C^2 C_J \left(\frac{x_{\text{ZPF}}}{\xi} \right)^2 (b^\dagger + b)^2 \right\} (a^\dagger + a)^4 \\ & = \left\{ -\frac{E_C}{12} + g_{42}(b^\dagger + b)^2 \right\} (a^\dagger + a)^4, \quad (\text{SI26}) \end{aligned}$$

where the first term contributes to the renormalization of the qubit frequency.

The energy of the shuttle $E(x_0 + \delta, p_m)$ is expressed as the sum of a kinetic $p_m/2m$ and an elastic $1/2 m \omega_m^2 (x_0 + \delta)^2$ contribution; it is quantized as $\omega_{m0} b^\dagger b$ where ω_{m0} is the bare mechanical frequency of the shuttle. The frequency ω_{m0} is renormalized partly by the

contribution proportional to $b^\dagger b$ from the following term

$$\begin{aligned}
-(E_{J1}(\hat{\delta}) + E_{J2}(\hat{\delta})) \cos \frac{\phi_b}{2} &\approx -(E_{J1} + E_{J2}) \cos \frac{\phi_b}{2} \\
&\quad - (E_{J2} - E_{J1}) \cos \frac{\phi_b}{2} \frac{x_{\text{ZPF}}}{\xi} (b^\dagger + b) \\
&\quad - \frac{1}{2} (E_{J1} + E_{J2}) \cos \frac{\phi_b}{2} \left(\frac{x_{\text{ZPF}}}{\xi} \right)^2 (b^\dagger + b)^2 \\
&= -(E_{J1} + E_{J2}) \cos \frac{\phi_b}{2} + g_{01} (b^\dagger + b) + g_{02} (b^\dagger + b)^2,
\end{aligned} \tag{SI27}$$

arising from the coupling to the qubit. We now expand the coefficients appearing in Eq. (SI22). The coefficient corresponding to the $(a^\dagger + a)$ term is

$$\begin{aligned}
&\left\{ -(E_{J1}(\hat{\delta}) + E_{J2}(\hat{\delta})) d(\hat{\delta}) \sin \frac{\phi_b}{2} \phi_{\text{ZPF}}(\hat{\delta}) \right\} (a^\dagger + a) \\
&\approx \left\{ -(E_{J2} - E_{J1}) \left(\frac{2E_C}{(E_{J1} + E_{J2}) \cos \frac{\phi_b}{2}} \right)^{\frac{1}{4}} \sin \frac{\phi_b}{2} \right. \\
&\quad - \frac{(3E_{J1} + E_{J2})(E_{J1} + 3E_{J2})}{4(E_{J1} + E_{J2})} \left(\frac{2E_C}{(E_{J1} + E_{J2}) \cos \frac{\phi_b}{2}} \right)^{\frac{1}{4}} \sin \frac{\phi_b}{2} \frac{x_{\text{ZPF}}}{\xi} (b^\dagger + b) \\
&\quad - \frac{(E_{J2} - E_{J1})}{32(E_{J1} + E_{J2})^2} (9E_{J1}^2 - 2E_{J1}E_{J2} + 9E_{J2}^2) \left(\frac{2E_C}{(E_{J1} + E_{J2}) \cos \frac{\phi_b}{2}} \right)^{\frac{1}{4}} \\
&\quad \left. \times \sin \frac{\phi_b}{2} \left(\frac{x_{\text{ZPF}}}{\xi} \right)^2 (b^\dagger + b)^2 \right\} (a^\dagger + a) \\
&= \left\{ -(E_{J2} - E_{J1}) \left(\frac{2E_C}{E_{J1} + E_{J2}} \right)^{\frac{1}{4}} \tan \frac{\phi_b}{2} \cos^{\frac{3}{4}} \frac{\phi_b}{2} \right. \\
&\quad - \frac{(3E_{J1} + E_{J2})(E_{J1} + 3E_{J2})}{4(E_{J1} + E_{J2})} \left(\frac{2E_C}{E_{J1} + E_{J2}} \right)^{\frac{1}{4}} \tan \frac{\phi_b}{2} \cos^{\frac{3}{4}} \frac{\phi_b}{2} \frac{x_{\text{ZPF}}}{\xi} (b^\dagger + b) \\
&\quad - \frac{(E_{J2} - E_{J1})}{32(E_{J1} + E_{J2})^2} (9E_{J1}^2 - 2E_{J1}E_{J2} + 9E_{J2}^2) \left(\frac{2E_C}{E_{J1} + E_{J2}} \right)^{\frac{1}{4}} \\
&\quad \left. \times \tan \frac{\phi_b}{2} \cos^{\frac{3}{4}} \frac{\phi_b}{2} \left(\frac{x_{\text{ZPF}}}{\xi} \right)^2 (b^\dagger + b)^2 \right\} (a^\dagger + a) \\
&= \{g_{10} + g_{11}(b^\dagger + b) + g_{12}(b^\dagger + b)^2\} (a^\dagger + a),
\end{aligned} \tag{SI28}$$

and finally the term with $(a^\dagger + a)^3$

$$\begin{aligned}
& \left\{ \frac{1}{6} (E_{J1}(\hat{\delta}) + E_{J2}(\hat{\delta})) d(\hat{\delta}) \sin \frac{\phi_b}{2} \phi_{\text{ZPF}}(\hat{\delta})^3 \right\} (a^\dagger + a)^3 \\
& \approx \left\{ \frac{1}{6} (E_{J2} - E_{J1}) \left(\frac{2E_C}{(E_{J1} + E_{J2}) \cos \frac{\phi_b}{2}} \right)^{\frac{3}{4}} \sin \frac{\phi_b}{2} \right. \\
& \quad + \frac{(E_{J1}^2 + 14E_{J1}E_{J2} + E_{J2}^2)}{24(E_{J1} + E_{J2})} \left(\frac{2E_C}{(E_{J1} + E_{J2}) \cos \frac{\phi_b}{2}} \right)^{\frac{3}{4}} \sin \frac{\phi_b}{2} \frac{x_{\text{ZPF}}}{\xi} (b^\dagger + b) \\
& \quad + \frac{(E_{J2} - E_{J1})}{192(E_{J1} + E_{J2})^2} (E_{J1}^2 - 82E_{J1}E_{J2} + E_{J2}^2) \left(\frac{2E_C}{(E_{J1} + E_{J2}) \cos \frac{\phi_b}{2}} \right)^{\frac{3}{4}} \\
& \quad \left. \times \sin \frac{\phi_b}{2} \left(\frac{x_{\text{ZPF}}}{\xi} \right)^2 (b^\dagger + b)^2 \right\} (a^\dagger + a)^3 \\
& = \left\{ \frac{1}{6} (E_{J2} - E_{J1}) \left(\frac{2E_C}{E_{J1} + E_{J2}} \right)^{\frac{3}{4}} \tan \frac{\phi_b}{2} \cos^{\frac{1}{4}} \frac{\phi_b}{2} \right. \\
& \quad + \frac{(E_{J1}^2 + 14E_{J1}E_{J2} + E_{J2}^2)}{24(E_{J1} + E_{J2})} \left(\frac{2E_C}{E_{J1} + E_{J2}} \right)^{\frac{3}{4}} \tan \frac{\phi_b}{2} \cos^{\frac{1}{4}} \frac{\phi_b}{2} \frac{x_{\text{ZPF}}}{\xi} (b^\dagger + b) \\
& \quad + \frac{(E_{J2} - E_{J1})}{192(E_{J1} + E_{J2})^2} (E_{J1}^2 - 82E_{J1}E_{J2} + E_{J2}^2) \left(\frac{2E_C}{E_{J1} + E_{J2}} \right)^{\frac{3}{4}} \\
& \quad \left. \times \tan \frac{\phi_b}{2} \cos^{\frac{1}{4}} \frac{\phi_b}{2} \left(\frac{x_{\text{ZPF}}}{\xi} \right)^2 (b^\dagger + b)^2 \right\} (a^\dagger + a)^3 \tag{SI29} \\
& = \{g_{30} + g_{31}(b^\dagger + b) + g_{32}(b^\dagger + b)^2\} (a^\dagger + a)^3.
\end{aligned}$$

Gathering all the terms, the full Hamiltonian is

$$\begin{aligned}
\hat{H} &= \omega_{p0} \left(a^\dagger a + \frac{1}{2} \right) + g_{21} \left(a^\dagger a + \frac{1}{2} \right) (b^\dagger + b) + g_{22} \left(a^\dagger a + \frac{1}{2} \right) (b^\dagger + b)^2 \\
& \quad + \omega_{m0} b^\dagger b - (E_{J1} + E_{J2}) \sin \frac{\phi_b}{2} + g_{01} (b^\dagger + b) + g_{02} (b^\dagger + b)^2 \\
& \quad - \frac{E_C}{12} (a^\dagger + a)^4 + g_{42} (a^\dagger + a)^4 (b^\dagger + b)^2 \\
& \quad + g_{10} (a^\dagger + a) + g_{11} (a^\dagger + a) (b^\dagger + b) + g_{12} (a^\dagger + a) (b^\dagger + b)^2 \\
& \quad + g_{30} (a^\dagger + a)^3 + g_{31} (a^\dagger + a)^3 (b^\dagger + b) + g_{32} (a^\dagger + a)^3 (b^\dagger + b)^2, \tag{SI30}
\end{aligned}$$

In the following, we neglect mixing of states outside the computational basis and therefore consider normal ordering the qubit operators $(a^\dagger + a)^3 \rightarrow 3(a^\dagger + a)$ and $(a^\dagger + a)^4 \rightarrow 12a^\dagger a$. A final mapping of bosonic operators onto Pauli matrices ($a^\dagger a \rightarrow 1/2(\sigma_z + 1)$ and $a^\dagger + a \rightarrow \sigma_x$)

allows us to write the final form of the Hamiltonian of the X2MON circuit as

$$\begin{aligned}
\hat{H} = & \frac{\omega_q}{2} \sigma_z + \omega_m b^\dagger b + g_{01}(b^\dagger + b) \\
& + [g_{21}(b^\dagger + b) + (g_{22} + 12g_{42})(b^\dagger + b)^2] \sigma_z \\
& + [(g_{10} + 3g_{30}) + (g_{11} + 3g_{31})(b^\dagger + b) + (g_{12} + 3g_{32})(b^\dagger + b)^2] \sigma_x
\end{aligned} \tag{SI31}$$

exhibiting both linear and quadratic coupling of the mechanical displacement to the σ_x and σ_z terms of the qubit. The relative strengths of the couplings can be tuned with the flux bias ϕ_b and also already in the fabrication stage of the device by choosing a suitable asymmetry of the Josephson energies of the junctions. Notably, the quadratic coupling to the σ_x component is weak compared to the other terms and can be disregarded in general. Here, the renormalized qubit and mechanical frequencies are

$$\begin{aligned}
\omega_q &= 2(\omega_{p0} - E_C), \\
\omega_m &= \omega_{m0} + (2g_{02} + g_{22} + 6g_{42}),
\end{aligned} \tag{SI32}$$

respectively.

For completeness, the full list of the coupling coefficients is

$$\begin{aligned}
\omega_{p0} &= \sqrt{8E_C(E_{J1} + E_{J2}) \cos \frac{\phi_b}{2}} \\
g_{21} &= \frac{d_0 x_{ZPF}}{2 \xi} \omega_{p0} \\
g_{22} &= \frac{1}{4} \left(\frac{x_{ZPF}}{\xi} \right)^2 \omega_{p0} \\
g_{42} &= \frac{1}{3e^2} E_C^2 C_J \left(\frac{x_{ZPF}}{\xi} \right)^2 \\
g_{01} &= -(E_{J2} - E_{J1}) \cos \frac{\phi_b}{2} \frac{x_{ZPF}}{\xi} \\
g_{02} &= -\frac{1}{2} (E_{J1} + E_{J2}) \cos \frac{\phi_b}{2} \left(\frac{x_{ZPF}}{\xi} \right)^2 \\
g_{10} &= -(E_{J2} - E_{J1}) \left(\frac{2E_C}{E_{J1} + E_{J2}} \right)^{\frac{1}{4}} \tan \frac{\phi_b}{2} \cos^{\frac{3}{4}} \frac{\phi_b}{2} \\
g_{11} &= -\frac{(3E_{J1} + E_{J2})(E_{J1} + 3E_{J2})}{4(E_{J1} + E_{J2})} \left(\frac{2E_C}{E_{J1} + E_{J2}} \right)^{\frac{1}{4}} \tan \frac{\phi_b}{2} \cos^{\frac{3}{4}} \frac{\phi_b}{2} \frac{x_{ZPF}}{\xi} \\
g_{12} &= -\frac{(E_{J2} - E_{J1})}{32(E_{J1} + E_{J2})^2} (9E_{J1}^2 - 2E_{J1}E_{J2} + 9E_{J2}^2) \left(\frac{2E_C}{E_{J1} + E_{J2}} \right)^{\frac{1}{4}} \\
&\quad \times \tan \frac{\phi_b}{2} \cos^{\frac{3}{4}} \frac{\phi_b}{2} \left(\frac{x_{ZPF}}{\xi} \right)^2 \\
g_{30} &= \frac{1}{6} (E_{J2} - E_{J1}) \left(\frac{2E_C}{E_{J1} + E_{J2}} \right)^{\frac{3}{4}} \tan \frac{\phi_b}{2} \cos^{\frac{1}{4}} \frac{\phi_b}{2} \\
g_{31} &= \frac{(E_{J1}^2 + 14E_{J1}E_{J2} + E_{J2}^2)}{24(E_{J1} + E_{J2})} \left(\frac{2E_C}{E_{J1} + E_{J2}} \right)^{\frac{3}{4}} \tan \frac{\phi_b}{2} \cos^{\frac{1}{4}} \frac{\phi_b}{2} \frac{x_{ZPF}}{\xi} \\
g_{32} &= \frac{(E_{J2} - E_{J1})}{192(E_{J1} + E_{J2})^2} (E_{J1}^2 - 82E_{J1}E_{J2} + E_{J2}^2) \left(\frac{2E_C}{E_{J1} + E_{J2}} \right)^{\frac{3}{4}} \\
&\quad \times \tan \frac{\phi_b}{2} \cos^{\frac{1}{4}} \frac{\phi_b}{2} \left(\frac{x_{ZPF}}{\xi} \right)^2.
\end{aligned} \tag{SI33}$$

Crucially, for symmetric Josephson junctions ($E_{J1} = E_{J2} \equiv E_J$), many of these couplings vanish, and we obtain $g_{01} = g_{10} = g_{12} = g_{21} = g_{30} = g_{32} = 0$, resulting in the Hamiltonian presented in the main text Eq. (5) with the notation $g_1 \equiv g_{11} + 3g_{31}$ and $g_2 \equiv g_{22} + 12g_{42}$ related to the couplings $g_1(b^\dagger + b)\sigma_x$ and $g_2(b^\dagger + b)^2\sigma_z$. For symmetric junctions, the

coefficients to these couplings are expressed as

$$\begin{aligned}
g_1 &= 2E_J \left(\frac{x_{\text{ZPF}}}{\xi} \right) \tan \frac{\phi_b}{2} \left[- \left(\frac{E_C}{E_J} \right)^{\frac{1}{4}} \cos^{\frac{3}{4}} \frac{\phi_b}{2} + \left(\frac{E_C}{E_J} \right)^{\frac{3}{4}} \cos^{\frac{1}{4}} \frac{\phi_b}{2} \right], \\
g_2 &= \left(\frac{x_{\text{ZPF}}}{\xi} \right)^2 \left[\sqrt{E_C E_J \cos \frac{\phi_b}{2}} + \frac{1}{3e^2} E_C^2 C_J \right].
\end{aligned} \tag{SI34}$$

APPROXIMATE STATE-SWAPPING HAMILTONIAN

We derive here the Hamiltonian H' given in Eq. (7) of the main text, by considering the effect of a flux modulation given by $\phi_b = \phi_{b0} \cos(\bar{\omega}t)$. As a result, the numerical factors appearing in the Hamiltonian given in Eq. (5) of the main text

$$\begin{aligned}
H &= \frac{\omega_q(t)}{2} \sigma_z + \omega_m(t) b^\dagger b \\
&\quad + g_1(t) (b^\dagger + b) \sigma_x + g_2(t) (b^\dagger + b)^2 \sigma_z
\end{aligned} \tag{SI35}$$

will be time-dependent. Up to second order in ϕ_{b0} , and first order in x_{ZPF}/ξ , it is possible to write them as

$$\begin{aligned}
\omega_q(t) &\simeq 2 \left(\omega_{p0} - E_C - \frac{\phi_{b0}^2 \omega_{p0}}{16} \frac{1 + \cos(2\bar{\omega}t)}{2} \right) \\
&= \bar{\omega}_q - \delta_q \cos(2\bar{\omega}t) \\
g_1(t) &\simeq \bar{g}_1 \cos(\bar{\omega}t) \\
\omega_m(t) &\simeq \omega_m(0) \\
g_2(t) &\simeq 0
\end{aligned} \tag{SI36}$$

where $\bar{\omega}_q = \omega_q|_{\phi_b=0} - \delta_q$, $\delta_q = \frac{\phi_{b0}^2 \omega_{p0}}{16}$, $\bar{g}_1 = E_J \left(\frac{E_C}{E_J} \right)^{1/4} \left(\sqrt{\frac{E_C}{E_J}} - 1 \right) \left(\frac{x_{\text{ZPF}}}{\xi} \right) \phi_{b0}$. With these approximations, we move to a rotating frame both for the qubit and the mechanical mode with the unitary transformation

$$U = \exp \left[-\frac{i}{2} \left\{ \bar{\omega}_q t - \frac{\delta_q}{2\bar{\omega}} \sin(2\bar{\omega}t) \right\} \sigma_z - i\omega_m b^\dagger b \right]. \tag{SI37}$$

In this frame the transformed Hamiltonian $H' = U^\dagger H U - U^\dagger \dot{U}$ can be written as

$$\begin{aligned}
H' &= \bar{g}_1 \cos(\bar{\omega}t) (b^\dagger e^{i\omega_m t} + b e^{-i\omega_m t}) [\cos \alpha(t) \sigma_x + \sin \alpha(t) \sigma_y] \\
&= \bar{g}_1 \cos(\bar{\omega}t) (b^\dagger e^{i\omega_m t} + b e^{-i\omega_m t}) (e^{-i\alpha(t)} \sigma_+ + e^{i\alpha(t)} \sigma_-)
\end{aligned} \tag{SI38}$$

with $\sigma_x = \sigma_+ + \sigma_-$, $\sigma_y = i(\sigma_+ - \sigma_-)$, and $\alpha(t) = \bar{\omega}_q t - \frac{\delta_q}{2\bar{\omega}} \sin(2\bar{\omega}t)$. Considering the relation

$$\exp[iz \sin \theta] = \sum_{k=-\infty}^{\infty} e^{ik\theta} J_k(z),$$

where $J_k(z)$ is the n -th order Bessel function, we can write H' as

$$H' = \bar{g}_1 \cos(\bar{\omega}t) (b^\dagger e^{i\omega_m t} + b e^{-i\omega_m t}) \left(e^{i\bar{\omega}_q t} \left[J_0\left(\frac{\delta_q}{2\bar{\omega}}\right) + J_1\left(\frac{\delta_q}{2\bar{\omega}}\right) e^{2i\bar{\omega}t} \dots \right] \sigma_+ + \text{h. c.} \right). \quad (\text{SI39})$$

For $\bar{\omega} = \bar{\omega}_q - \omega_m$, invoking the rotating wave approximation and neglecting non-resonant terms, Eq. (SI39) can be written as

$$H' = \bar{g}_1 J_0\left(\frac{\delta_q}{2\bar{\omega}}\right) (b^\dagger \sigma_- + \text{h. c.}). \quad (\text{SI40})$$

With $\bar{g}_1 J_0\left(\frac{\delta_q}{2\bar{\omega}}\right) = g_{\text{sw}}$ this is the expression given in Eq. (7) of the main text.

* francesco.massel@usn.no

- [1] S. M. Girvin, École d'été Les Houches (2011).
- [2] U. Vool and M. Devoret, International Journal of Circuit Theory and Applications **45**, 897 (2017).
- [3] V. Ambegaokar and A. Baratoff, Physical Review Letters **10**, 486 (1963).
- [4] J. M. Martinis, Les Houches **79**, 487 (2004).
- [5] R. Landauer, IBM Journal of Research and Development **1**, 223 (1957).